



The different sensitivities of aerosol optical properties to particle concentration, humidity, and hygroscopicity between the surface level and the upper boundary layer in Guangzhou, China

Xiaoai Jin ^a, Zhanqing Li ^{b,*}, Tong Wu ^a, Yuying Wang ^c, Yafang Cheng ^d, Tianning Su ^b, Jing Wei ^a, Rongmin Ren ^a, Hao Wu ^e, Shangze Li ^a, Dongmei Zhang ^a, Maureen Cribb ^b

^a State Key Laboratory of Remote Sensing Science, College of Global Change and Earth System Science, Beijing Normal University, Beijing 100875, China

^b Department of Atmospheric and Oceanic Science and ESSIC, University of Maryland, College Park, MD, USA

^c Key Laboratory for Aerosol-Cloud-Precipitation of China Meteorological Administration, School of Atmospheric Physics, Nanjing University of Information Science and Technology, Nanjing 210044, China

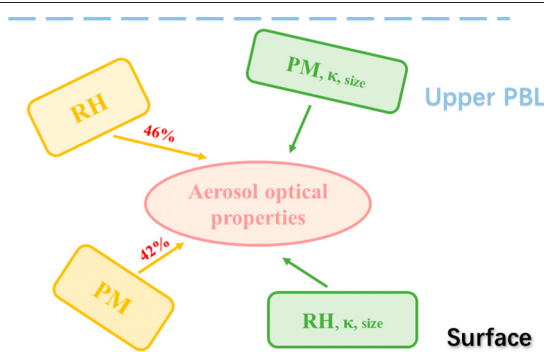
^d Minerva Research Group, Max Planck Institute for Chemistry, 55128 Mainz, Germany

^e College of Electronic Engineering, Chengdu University of Information Technology, Chengdu 610225, China

HIGHLIGHTS

- The impact of aerosol liquid water on aerosol scattering is identified and differentiated with those of related factors;
- The joint effect of the multi-factors render incoherent, even opposite diurnal pattern of aerosol scattering at ground and 532 m;
- Aerosol mass plays a more significant role in aerosol scattering than humidity on ground, while the opposite is true at 532m.

GRAPHICAL ABSTRACT



ARTICLE INFO

Article history:

Received 26 April 2021

Received in revised form 23 August 2021

Accepted 25 August 2021

Available online 30 August 2021

Editor: Jianmin Chen

Keywords:

Aerosol liquid water content (ALWC)

Aerosol backscattering coefficient

Aerosol hygroscopicity

PM_{2.5}

ABSTRACT

This study investigates the impact of aerosol liquid water content (ALWC) and related factors, i.e., relative humidity (RH), aerosol mass concentration (PM_{2.5}), and aerosol hygroscopicity, on aerosol optical properties, based on field measurements made in the Pearl River Delta (PRD) region of China at the surface (1 November 2019 to 21 January 2020) and in the upper boundary layer (the 532-m Guangzhou tower from 1 February to 21 March 2020). In general, temporal variations in the ambient aerosol backscattering coefficient (β_p) and ALWC followed each other. However, the surface β_p and 532-m β_p had generally opposite diurnal variation patterns, caused by dramatic differences in PM_{2.5} and ambient RH between the surface and the upper boundary layer. The ambient 532-m RH was systematically higher than the surface RH, with the latter having a much pronounced diurnal cycle than the former. The surface PM_{2.5} concentration was systematically higher than the PM_{2.5} concentration at 532 m, and their diurnal cycle patterns were overall opposite. These dramatic differences reveal that the atmospheric variables, i.e., ambient RH and the PM_{2.5} concentration in the upper boundary layer, cannot be directly represented by the same variables at the surface. Vertical variability should be considered. Clear differences in the sensitivities of aerosol light scattering to ambient RH, PM_{2.5}, and aerosol hygroscopicity between the two levels were found and examined. Aerosol chemical composition played a minor role in causing the differences between the two levels. In particular, β_p was more sensitive to PM_{2.5} at the surface

* Corresponding author.

E-mail address: zhanqing@umd.edu (Z. Li).

level but more to the ambient RH in the upper boundary layer. The larger contribution of aerosol loading to the variability in β_p at the surface implies that local emission controls can decrease β_p and further improve atmospheric visibility effectively at the surface during winter in the PRD region.

© 2021 Elsevier B.V. All rights reserved.

1. Introduction

Severe air pollution in China has drawn widespread public attention in recent years because it is detrimental to human health and influences regional weather and climate (Zheng et al., 2015; Wang et al., 2016; Li et al., 2016; Guo et al., 2017; Fan et al., 2018; Hu et al., 2020; Su et al., 2020a). The degradation in visibility is the most apparent impact, caused by light extinction by particles in the atmosphere, which may seriously affect people's daily lives through all forms of transportation, e.g., driving, sailing, and aviation (Chen et al., 2014; Huang et al., 2014; Ma et al., 2014). However, aerosol direct radiative effects remain highly uncertain due to the incomplete understanding of complex aerosol particle optical and chemical properties (Cheng et al., 2006; Tao et al., 2012; IPCC, 2013; Guo et al., 2019; Su et al., 2020b).

The radiative effects of aerosols are affected by aerosol loading, composition, and mixing state. The latter two parameters dictate the aerosol hygroscopic property, which, together with relative humidity (RH), determines the aerosol liquid water content (ALWC) in aerosol particles. The light extinction, scattering, and absorption by aerosol particles are most significantly influenced by aerosol loading (Gobbi et al., 2003; Pierangelo et al., 2004; Wang et al., 2005). During the 2015 China Victory Day parade in Beijing, the Chinese government implemented strict emission control measures, effectively reducing aerosol mass concentrations and improving visibility (Wang et al., 2017). Zhang et al. (2010) found that the aerosol extinction coefficient (σ_{ep}) and the scattering coefficient (σ_{sp}) of dust aerosols both correlate well with aerosol mass concentration. However, aerosol loading is influenced by liquid water content (Tao et al., 2014; Kuang et al., 2016). Aerosol particles can take up water as the ambient RH increases, impacting aerosol optical properties, especially particle light scattering, by changing the particle size and shape. The ALWC can account for more than 50% of the particle mass under high ambient RH conditions (Cheng et al., 2008a; Bian et al., 2014; Tan et al., 2017; Jin et al., 2020). The ALWC can also facilitate the formation of secondary aerosols (SA) by speeding up the transformation of sulfur dioxide (SO_2) to sulfate, the uptake coefficient of nitrogen pentoxide (N_2O_5), and oxidation of organics through multiple chemical reactions, consequently facilitating the formation of air pollution and degrading visibility (Wehner et al., 2008; Surratt et al., 2007; Hennigan et al., 2008; H. Su et al., 2020).

Several field campaigns, laboratory experiments, and modeling efforts have addressed the influences of hygroscopic growth on aerosol optical properties. Covert et al. (1972) studied the relationship between light scattering and aerosol chemical composition and humidity, based on laboratory experiments, finding that light scattering is increased by a factor of three when the RH level was 90%. Tao et al. (2014) demonstrated the significantly different diurnal patterns of the ambient single-scattering albedo (ω) and ω measured at the dry state, both of which were highly sensitive to the ambient RH. Yoon and Kim (2006) reported that σ_{sp} was significantly enhanced under ambient RH conditions compared to dry conditions, based on RH and σ_{sp} profiles under ambient and low RH conditions. The dependence of aerosol optical properties on RH and direct radiative forcing in the surface boundary layer was investigated in the Pearl River Delta (PRD) region (Cheng et al., 2008a). Cheng et al. (2008b) also found that the water uptake of particles can contribute 50–60% to σ_{ep} at an RH level of 90% and that sulfate, carbonaceous material, and water all played very important roles in degrading visibility at Xinken in the PRD region. Zieger et al. (2013) studied the effect of aerosol hygroscopic growth on σ_{sp} by comparing measurements

from five European sites and found significant discrepancies between observations and modeling due to the inappropriate implementation of hygroscopic growth in the model. These all demonstrate that the degradation in visibility is related to the interaction between water uptake and hygroscopic aerosol particles except for that caused by the particles alone.

In summary, most previous studies have mainly studied the impact of related factors, such as aerosol mass, aerosol hygroscopic growth, aerosol chemical composition, and ambient RH, on aerosol optical properties separately. A thorough understanding of the relative importance of each of these related factors in controlling aerosol optical properties is lacking. Moreover, most previous studies have focused on the impact of aerosol particle mass and aerosol hygroscopic growth on aerosol optical properties at the surface level. With the total column of aerosol properties as input, the aerosol radiative forcing has been simulated in numerous studies (Ding et al., 2016; Zhou et al., 2018). The vertical profiles of aerosol properties play a critical role in cloud formation (Hu et al., 2021) and aerosol radiative effects (Su et al., 2020b). However, previous model simulations of studies often suffered from lacking the aerosol vertical structure data. By using comprehensive field measurements, this study investigates the association between aerosol backscattering coefficient (β_p) and ALWC and related factors (ambient RH, aerosol mass concentration, and aerosol hygroscopicity) and the relative importance of each factor in influencing β_p . Further compared are their differences between the surface level and the upper boundary layer. We demonstrate the clear sensitivity of aerosol light scattering to ambient RH, aerosol mass concentration ($\text{PM}_{2.5}$), and aerosol hygroscopicity.

2. Data and measurements

2.1. Observation station

To understand aerosol formation and growth, their interactions with the boundary layer, and impact on air quality, a winter field campaign was carried out from 1 November 2019 to 21 March 2020 at the Guangzhou Meteorological Bureau (GMB) in Guangzhou, a megacity located in the PRD region of China. The GMB station (23.01°N, 113.33°E) is located in the southwest suburb of Guangzhou near China's largest amusement park called Chang Long Paradise (Fig. 1). This observation site is influenced by a variety of urban pollutants from small factories, traffic, and cooking. The field campaign was conducted at both the surface level (1 November 2019 to 21 January 2020, first phase) and at the 532-m Guangzhou tower (1 February to 21 March 2020, second phase) located ~10 km north of the ground station. The planetary boundary layer (PBL) height ranged from 300 m to 1.5 km during the experiment (Fig. S1). During the cold season (November to March), diurnal variations in PBL depth generally range from 400 m to 900 m over the PRD region (Yang et al., 2013; Deng et al., 2014; Guo et al., 2016; Su et al., 2017, 2018). Fig. S2 shows the potential temperature (θ) at the surface and at 532 m. The surface θ was systematically higher than that at 532 m during daytime and slightly lower than that at 532 m at night. The daytime θ differences indicate that observations at 532 m were below the top of the mixing layer. Given the decay of the mixing layer during the nighttime, observations at 532 m were in the residual layer (Fig. S3). During the transition from the mixing layer to the residual layer, aerosol properties do not significantly change (Nilsson et al., 2001; Venzac et al., 2009). Data collected in the presence of the residual layer were thus not excluded from our analyses. Tower measurements

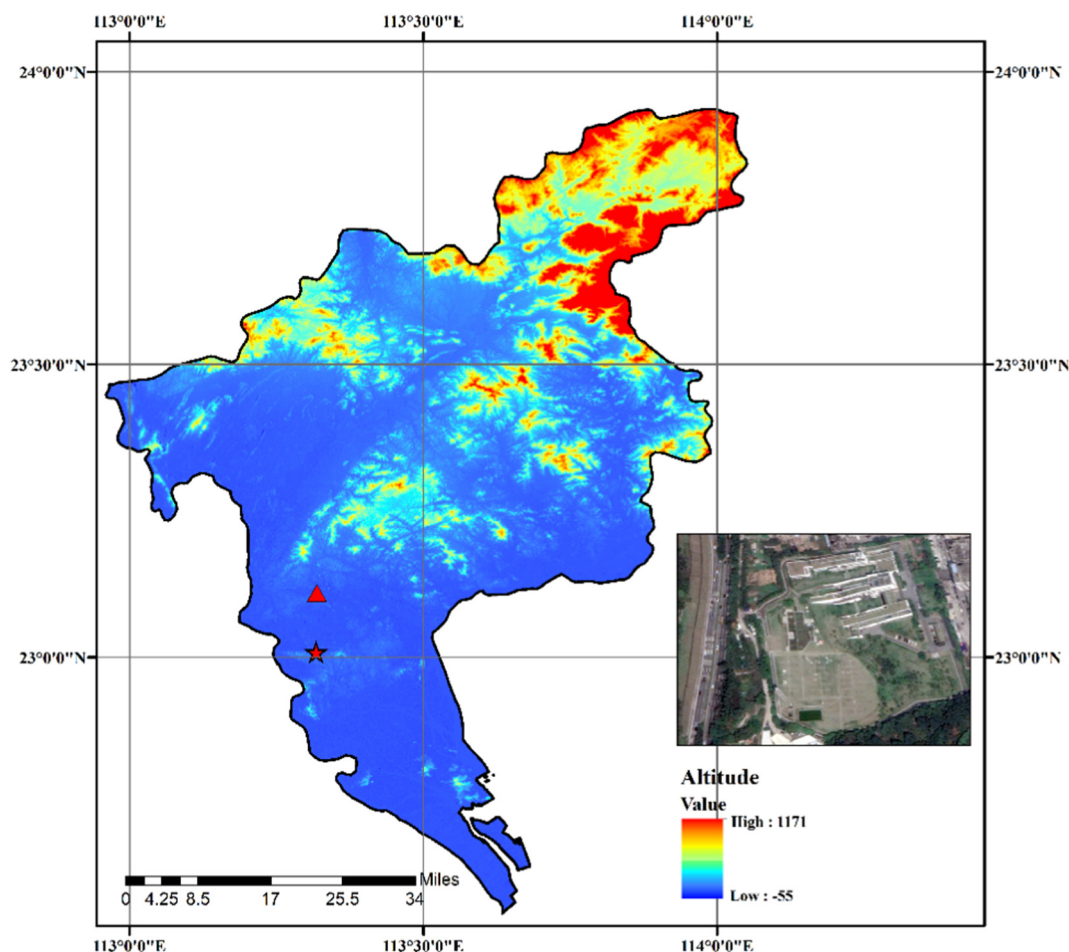


Fig. 1. Locations of the observation station at the surface level (red star) and the 532 m Guangzhou tower (red triangle) and the terrain of Guangdong province (colored background, unit: m). The inset figure shows an image of the site at the surface and its surroundings. (For interpretation of the references to color in this figure legend, the reader is referred to the web version of this article.)

made at 532 m can generally represent air quality conditions in the upper part of the PBL during our experiment.

2.2. Instrumentation

Ground-based observations were conducted in an air-conditioned mobile container with a stable temperature environment ($\sim 20\text{--}25\text{ }^{\circ}\text{C}$). A scanning mobility particle sizer (SMPS), a humidified nephelometer system, and an aerosol chemical speciation monitor (ACSM) were installed inside the container. A $\text{PM}_{2.5}$ cyclone (model URG-2000-30ED) was affixed to the top of the container in front of the sampling inlet to remove particles larger than $2.5\text{ }\mu\text{m}$. After going through the $\text{PM}_{2.5}$ cyclone, the sampled air was dried (below 30% RH) by a dryer system, comprised of a silica gel tube and a Nafion dryer (model PD-70T-24ss, Perma Pure Inc., USA), and streamed to different instruments. During the field campaign at the Guangzhou tower, an ACSM was installed in a sampling room located on a platform, set up in the same way as on the ground. Meteorological variables, including wind speed (WS), wind direction (WD), temperature (T), and RH, were measured by a Li-COR 7500A system. Quality-controlled $\text{PM}_{2.5}$ data at the ground level were obtained from real-time PM observations released by the China National Environmental Monitoring Centre. $\text{PM}_{2.5}$ at 532 m was measured by a tapered element oscillating microbalance monitor. In this study, all times are local times (LTs) in Beijing (UTC + 8 h).

The ACSM was used to measure the aerosol chemical composition of non-refractory submicron particles in real time. It provides composition information about particulate ammonium (NH_4^+), sulfate (SO_4^{2-}), nitrate

(NO_3^-), chloride (Cl^-), and organics (Org) at a 15-min time resolution. After the sampled air was dried to below 30% RH, it went into a high-vacuum system through a particle aerodynamic lens that focused sub-micron aerosols ($\sim 0.04\text{--}2.5\text{ }\mu\text{m}$ aerodynamic diameter) into a narrow beam. It was then directed to a resistance-heated particle vaporizer, operating at $\sim 600\text{ }^{\circ}\text{C}$, installed in the ionization chamber of the mass spectrometer where non-refractory components on the particle flash vaporized on impact. The vaporized constituents were then ionized by electron impact and analyzed using a quadrupole mass spectrometer. Regular calibration of the ACSM with pure ammonium nitrate was used to determine its ionization efficiency following the procedures detailed by Jimenez et al. (2003). Ng et al. (2011) and Sun et al. (2012) provide more detailed descriptions of the ACSM.

Aerosol vertical optical profiles, including σ_{ep} , β_{p} , and the particle linear depolarization ratio, were measured by a micro-pulse lidar (MPL-4B, Sigma Space Corp.). Wu et al. (2020) describe in detail the MPL used in this study. In brief, the MPL is comprised of a low-energy laser with a high pulse-repetition rate (2500 Hz) at 532 nm, providing continuous profile data with a time resolution of 60 s and a vertical resolution of 30 m (Huang et al., 2010). Since there was no humidified nephelometer on the tower platform, β_{p} at 509 m measured by the MPL ($\beta_{\text{p, RH, MPL}}$) was used for evaluation because of the tower measurements at 532 m.

A humidified nephelometer system (Aurora 3000, Ecotech) with a time resolution of 1 min measured aerosol optical properties (i.e., σ_{sp} and β_{p} at 525 nm) at the ground level. The σ_{sp} and the β_{p} were measured after drying ($\sigma_{\text{sp, dry, Hneph}}$; $\beta_{\text{p, dry, Hneph}}$), while the aerosol vertical optical property profiles retrieved by the MPL were made

under ambient RH conditions. Therefore, based on the hygroscopic enhancement factor measured by the humidified nephelometer system, $\beta_{p, \text{dry}}$ values at the surface were transformed into those under ambient RH conditions ($\beta_{p, \text{RH, Hneph}}$) and used for evaluation at the surface (Fig. S4).

3. Methodology

3.1. Hygroscopicity parameter

For a multicomponent particle, the hygroscopicity parameter κ , based on the Zdanovskii–Stokes–Robinson (ZSR) mixing rule (Stokes and Robinson, 1966), can be expressed as the sum of the contributions of each aerosol component:

$$\kappa = \sum_i \varepsilon_i \kappa_i, \quad (1)$$

where ε_i and κ_i are the volume fraction and hygroscopicity parameter of the i th aerosol component, respectively. The parameter κ can also be expressed as the sum of the contributions of Org and inorganics because submicron aerosols can be mainly divided into organic and inorganic species (Carbone et al., 2013; Zieger et al., 2017). The ACSM provides the mass concentrations of Org and inorganics, including SO_4^{2-} , NO_3^- , NH_4^+ , and Cl^- . The ion-pairing scheme (Gysel et al., 2007) was used to calculate the volume fractions of inorganic species:

$$\begin{aligned} n_{\text{NH}_4\text{NO}_3} &= n_{\text{NO}_3^-}, \\ n_{\text{NH}_4\text{HSO}_4} &= \min(2n_{\text{SO}_4^{2-}} - n_{\text{NH}_4^+} + n_{\text{NO}_3^-}, n_{\text{NH}_4^+} - n_{\text{NO}_3^-}), \\ n_{(\text{NH}_4)_2\text{SO}_4} &= \max(n_{\text{NH}_4^+} - n_{\text{NO}_3^-} - n_{\text{SO}_4^{2-}}, 0), \\ n_{\text{H}_2\text{SO}_4} &= \max(0, n_{\text{SO}_4^{2-}} - n_{\text{NH}_4^+} + n_{\text{NO}_3^-}), \\ n_{\text{HNO}_3} &= 0, \end{aligned} \quad (2)$$

where n represents the mole numbers of each inorganic ion and species, and “min” and “max” represent the minimum and maximum values, respectively. Here, the volumes of black carbon (BC) and mineral dust were not taken into account in calculating the volume fractions because BC and mineral dust particles have little impact on the κ calculation (Malm et al., 2009; Levin et al., 2014). In this study, the κ values of the inorganic species, sulfuric acid (H_2SO_4), ammonium sulfate ($(\text{NH}_4)_2\text{SO}_4$), ammonium hydrogen sulfate (NH_4HSO_4), ammonium nitrate (NH_4NO_3), and organics were 1.19, 0.48, 0.56, 0.58, and 0.1, respectively (Petters and Kreidenweis, 2007; Wex et al., 2009; Nguyen et al., 2016).

3.2. ALWC simulations

The thermodynamic equilibrium model ISORROPIA II (Fountoukis and Nenes, 2007), with inorganic species (NH_4^+ , SO_4^{2-} , NO_3^- , and Cl^-) measured by the ACSM and measured ambient RH and T values as input, was used to compute ALWC. In this study, the model was set up to the metastable phase state and the reverse mode due to a lack of data about gaseous ammonia.

The model ISORROPIA II assumes that aerosol hygroscopicity has no effect on ambient vapor pressure and neglects the Kelvin effect in the κ -Köhler theory (Fountoukis and Nenes, 2007). This may have an effect on the water uptake of the Aitken mode, but the influence is overall small (Zieger et al., 2017). Consequently, in this model, the water activity (a_w), defined as the effective mole fraction of water, is thus equal to the ambient RH (Seinfeld and Pandis, 2006):

$$a_w = \text{RH}. \quad (3)$$

The ALWC can then be derived according to the ZSR mixing rule (Stokes and Robinson, 1966),

$$\text{ALWC} = \sum_i \frac{M_i}{m_{0i}(a_w)}, \quad (4)$$

where M_i and $m_{0i}(a_w)$ represent the mole concentration and the corresponding molality of the binary solution of the i th species under the same a_w with a complex solution, respectively. The ALWC simulated by the ISORROPIA II contains uncertainties incurred for not accounting for the contribution of organics. Thus, the simulated ALWC was compared with ALWC derived from the measurements of a humidified nephelometer system, which agree well (Fig. S5).

3.3. The contribution of RH, $\text{PM}_{2.5}$, and κ to the variabilities in β_p

Based on the assumption that β_p is affected by ambient RH, mass loading (represented by $\text{PM}_{2.5}$ here), and κ , β_p can be expressed as a function of these parameters (Huang and Yi, 1991; Cui et al., 2021):

$$\beta_p = f(\text{RH}, \text{PM}, \kappa). \quad (5)$$

The $\text{PM}_{2.5}$ mass concentration and κ can both be set to constant values, e.g., $\text{PM}_{2.5} = 50 \mu\text{g m}^{-3}$ and $\kappa = 0.3$, to screen out ambient RH and β_p values under the same $\text{PM}_{2.5}$ and κ conditions based on all observational data. The absolute change in β_p due to ambient RH can be calculated as

$$\Delta\beta_p(\text{RH}) = f(\text{RH}, \text{PM}_0, \kappa_0), \quad (6)$$

where PM_0 and κ_0 represent constant values of $\text{PM}_{2.5}$ mass concentration and κ . Similarly, the absolute change in β_p due to $\text{PM}_{2.5}$ mass concentration and κ can also be calculated. In this study, the gradient of $\text{PM}_{2.5}$, ambient RH, and κ are set to $5 \mu\text{g m}^{-3}$, 1%, and 0.1, respectively. The change in β_p due to ambient RH, $\text{PM}_{2.5}$ mass concentration, and κ together can then be expressed as

$$\Delta\beta_p(\text{RH}, \text{PM}, \kappa) = a \cdot \Delta\beta_p(\text{RH}) + b \cdot \Delta\beta_p(\text{PM}) + c \cdot \Delta\beta_p(\kappa). \quad (7)$$

The coefficients a , b , and c can be derived through multiple linear regression. The coefficients a , b , and c are 0.32, 0.42, and 0.36 at the surface, respectively, and 0.82, 0.67, and 0.72 at the 532-m level, respectively. Finally, the contributions of the three factors to the variability in β_p can be calculated:

$$\begin{aligned} F_{\text{RH}} &= \frac{1}{m} \sum_{j=1}^m \frac{a \cdot \Delta\beta_p(\text{RH})_j}{a \cdot \Delta\beta_p(\text{RH})_j + b \cdot \Delta\beta_p(\text{PM})_j + c \cdot \Delta\beta_p(\kappa)_j}, \\ F_{\text{PM}} &= \frac{1}{m} \sum_{j=1}^m \frac{b \cdot \Delta\beta_p(\text{PM})_j}{a \cdot \Delta\beta_p(\text{RH})_j + b \cdot \Delta\beta_p(\text{PM})_j + c \cdot \Delta\beta_p(\kappa)_j}, \\ F_{\kappa} &= \frac{1}{m} \sum_{j=1}^m \frac{c \cdot \Delta\beta_p(\kappa)_j}{a \cdot \Delta\beta_p(\text{RH})_j + b \cdot \Delta\beta_p(\text{PM})_j + c \cdot \Delta\beta_p(\kappa)_j}, \end{aligned} \quad (8)$$

where m represents the length of the sample series.

4. Results and discussion

4.1. Overview

Figs. 2 and 3 show the temporal variations in the main aerosol properties during the experiment at the ground level and at 532 m on the tower. There were four main haze events observed, manifested as a rapid accumulation of particles at the ground level (Fig. 2a). However, no pollution event was observed at the 532-m tower level, with low $\text{PM}_{2.5}$ values throughout the entire experiment (Fig. 3a). The average mass concentration at the ground level was $45 \pm 26 \mu\text{g m}^{-3}$, which was much higher than that at 532 m ($18 \pm 11 \mu\text{g m}^{-3}$). This is likely because the aerosol mass concentration usually decreases with altitude (Su et al., 2018; Wei et al., 2021). It is also linked with the impact of the nation-wide shutdown due to the coronavirus (COVID-

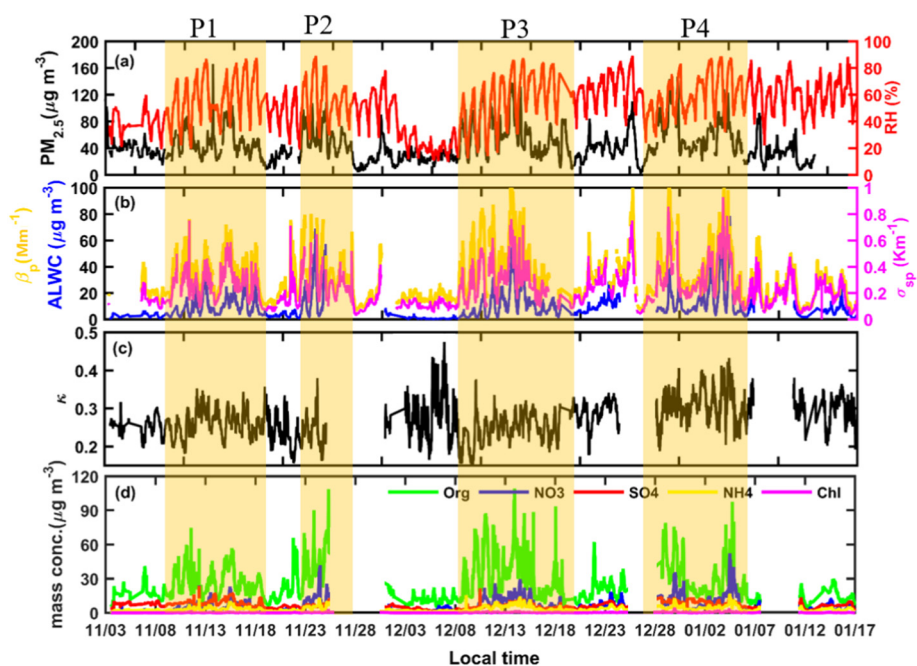


Fig. 2. Time series of (a) $PM_{2.5}$ mass concentration and ambient relative humidity (RH), (b) aerosol liquid water content (ALWC), aerosol total scattering coefficient (σ_{sp}), and aerosol backscattering coefficient (β_p), (c) aerosol hygroscopicity (κ), and (d) aerosol chemical composition at the ground level during the experiment. Four pollution episodes (segments of the time series with a yellow background) are selected for further examination. (For interpretation of the references to color in this figure legend, the reader is referred to the web version of this article.)

19) pandemic that was taking place in China, leading to a sharp decline in $PM_{2.5}$ both at the ground level and at 532 m during the second phase of the field campaign (1 February to 21 March 2020, Fig. S6). Figs. 2a and 3a also show time series of the ambient RH at the ground level and at 532 m. The ambient RH at the ground level varied more dramatically than the ambient RH at 532 m. The temperature at 532 m was systematically lower than that at the ground level, with T not changing much during the two phases of the field campaign (Fig. S7).

Fig. 2b shows time series of ALWC and β_p at the ground level. The temporal variation in β_p was generally consistent with ALWC, indicating that aerosol hygroscopic growth can change the particle size, modifying the aerosol backscattering (Zieger et al., 2013; Kuang et al., 2016). $PM_{2.5}$ and β_p also had similar trends (Fig. 2a and b). Because $PM_{2.5}$ concentrations were measured after drying during the experiment, thus representing the mass concentrations of dry aerosol particles, this demonstrates the important impact of the accumulation of dry

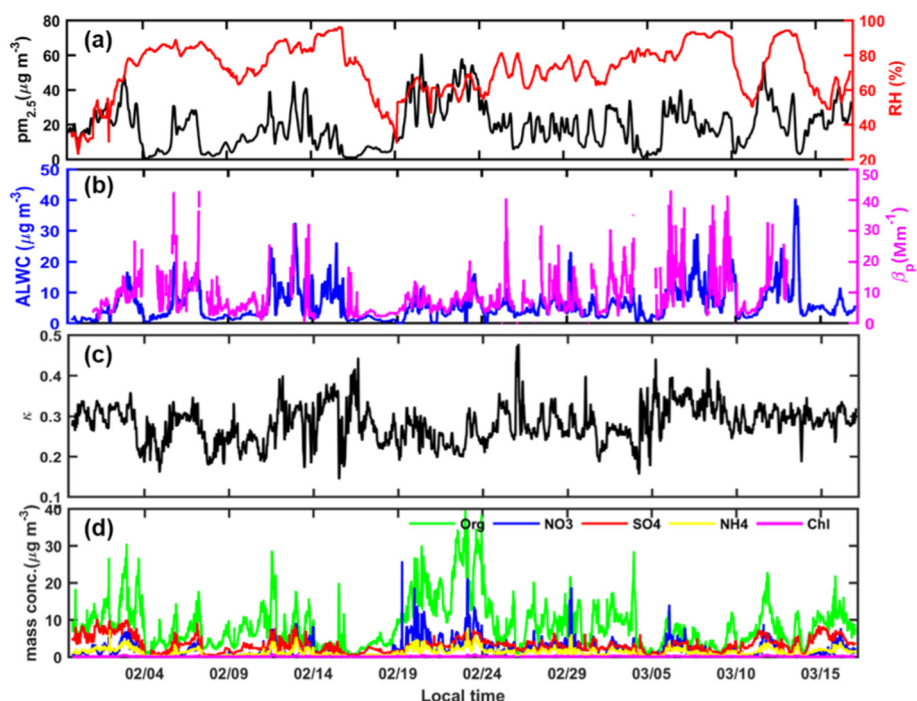


Fig. 3. Same as Fig. 2 except at the 532-m level on the tower. In (b), the aerosol total scattering coefficient is not shown.

aerosol particles on light scattering. Fig. S8 shows time series of the particle number size distributions (PNSDs) during the two observational phases at the surface. The average PNSDs during the two observational phases had similar patterns, with one peak at ~ 20 nm and one small peak at ~ 100 nm (Fig. S9a). Moreover, the average PNSD during the first phase showed much higher number concentrations than during the second phase due to the impact of the COVID-19 lockdown, as expected (Fig. S9a). To better compare differences in the size distribution between the two observational phases, normalized PNSDs were analyzed. On average, the normalized PNSDs had similar patterns. The peaks during the second phase were slightly smaller than during the first phase (Fig. S9b). These results illustrate that mission sources remained essentially the same during the two phases. Similar to the situation at the surface level, high values of β_p at 532 m were usually associated with correspondingly high ALWC values (Fig. 3b), suggesting the important influence of aerosol hygroscopicity on light scattering both at the ground level and at 532 m. MPL-retrieved β_p values associated with very high RH values are not considered in the subsequent analysis because of the high probability of cloud contamination. At the ground level, average ALWC and β_p values were $12 \pm 10 \mu\text{g m}^{-3}$ and $30 \pm 16 \text{ Mm}^{-1}$, respectively. At 532 m, average ALWC and β_p values were $4 \pm 3 \mu\text{g m}^{-3}$ and $7.2 \pm 4.2 \text{ Mm}^{-1}$, respectively. Note that the ambient RH at 532 m remained relatively high, while ALWC values at 532 m were much lower than at the ground level. This suggests that ALWC cannot easily increase during clean periods, even though high RH conditions provide sufficient water for the uptake of water by aerosol particles. Figs. 2a and b and 3a and b also show that the increases in β_p were synchronous with the increases in aerosol mass concentration and ambient RH. On average, at the ground level, β_p increased from 10 to 75 Mm^{-1} as $\text{PM}_{2.5}$ increased from 12 to $89 \mu\text{g m}^{-3}$, and ambient RH increased from 22% to 85%. These results indicate that the increase in aerosol mass concentration, particle size, and ambient RH all play a role in the increase in β_p .

Figs. 2d and 3d show the mass concentrations of aerosol components (Org, NH_4^+ , SO_4^{2-} , NO_3^- , and Cl^-) at the ground level and at 532 m, respectively. At the ground level and at 532 m, Org were overall the dominant species in $\text{PM}_{2.5}$, accounting for 58% and 57%, followed by sulfate accounting for 18% and 20%, respectively (Fig. S10). Figs. 2c and 3c show the hygroscopicity parameter κ derived from the chemical

composition at the ground level and at 532 m, with average κ values of 0.28 (ranging from 0.14 to 0.6) and 0.27 (ranging from 0.16 to 0.58), respectively. These results indicate that the meteorological conditions and emission sources did not change much during the observation period, suggesting that it is of significance to compare the effects of ALWC and related factors (ambient RH, aerosol mass, and hygroscopicity) on β_p between the ground level and 532 m. Fig. 2 shows that κ also increased as the $\text{PM}_{2.5}$ mass concentration and ambient RH increased. This is likely because, along with the increase in ambient RH, aerosol particles can take up water, facilitating the formation of SA and increasing aerosol hygroscopicity (Martin, 2000; Cheng et al., 2016; Wang et al., 2016). The newly formed SA are beneficial toward enhancing aerosol hygroscopicity because they are usually highly aged. This can further enhance the uptake of water by aerosols, facilitating the formation of pollution. β_p thus increases, and atmospheric visibility decreases. This positive feedback also occurred at 532 m. These results suggest that aerosol hygroscopicity also has a large influence on aerosol optical properties except for the ambient RH and aerosol mass concentration.

4.2. Diurnal variations at the ground level and at 532 m

Fig. 4a and b show the diurnal variations in β_p and ALWC at the ground level, respectively. In general, the diurnal cycles of ALWC and β_p were similar. Both ALWC and β_p diurnal cycles had clear peaks ($16 \mu\text{g m}^{-3}$ and 36 Mm^{-1}) in the early morning and valleys ($4 \mu\text{g m}^{-3}$ and 23 Mm^{-1}) in the afternoon. The diurnal cycles of ALWC and β_p at 532 m also showed a similar pattern, with a clear peak ($6 \mu\text{g m}^{-3}$ and 10 Mm^{-1}) at noon (1230 LT and 1130 LT, respectively), suggesting that ALWC plays an important role in influencing aerosol optical properties both at the surface and in the upper boundary layer, especially under high ambient RH conditions (Fig. 4c and d). Note that the times when the peak and valley appeared in the β_p diurnal cycle (0100 LT and ~ 1700 LT) were different from those in the ALWC diurnal cycle (0600 LT and ~ 1600 LT) at the surface level. As shown in Fig. 5a and c, the sharp decline in $\text{PM}_{2.5}$ from $52 \mu\text{g m}^{-3}$ to $36 \mu\text{g m}^{-3}$ at 2300 LT led to the peak in β_p appearing earlier than of the peak in ALWC. The continuous decrease in $\text{PM}_{2.5}$ in the afternoon also resulted in the valley in β_p appearing

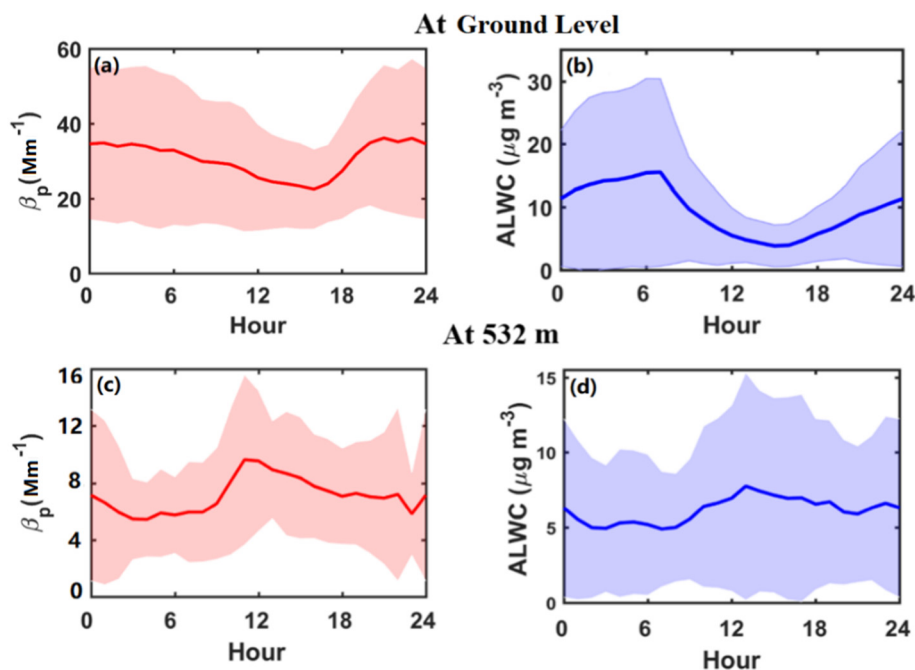


Fig. 4. Diurnal variations in aerosol backscattering coefficient (β_p , left panels) and aerosol liquid water content (ALWC, right panels) at the ground level (top panels) and at 532 m (bottom panels). The shaded areas represent standard deviations.

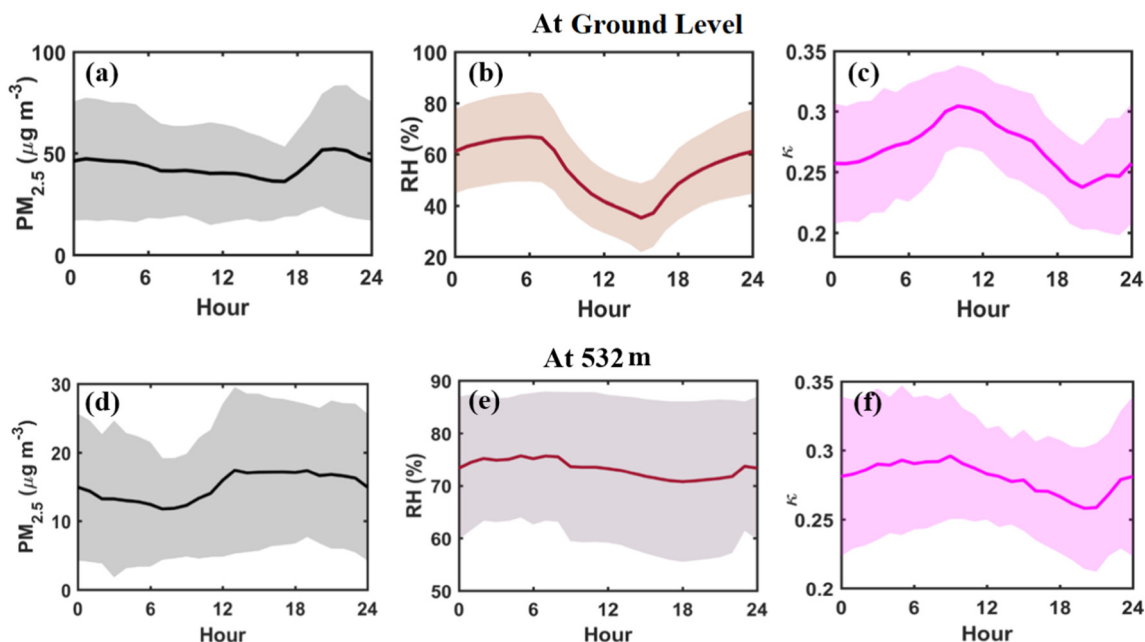


Fig. 5. Diurnal variations in $PM_{2.5}$ mass concentration (left panels), relative humidity (RH, middle panels), and aerosol hygroscopicity (κ , right panels) at the ground level (top panels) and at 532 m (bottom panels). The shaded areas represent standard deviations.

later than the valley in ALWC. These results indicate that the surface β_p was not only significantly affected by aerosol hygroscopic growth but also affected by the accumulation of fine-mode particles. The surface ALWC and ambient RH had similar diurnal variations, with peaks at 0600 LT and valleys at 1600 LT (Figs. 4b and 5b), indicating that ambient RH played a key role in determining the diurnal variation in surface ALWC.

The diurnal variations in ALWC and β_p at the surface and at 532 m differed. At the ground level, higher values of ALWC and β_p were seen at night, and lower values were seen in the daytime, while at 532 m, the opposite occurred. The dramatic differences in the diurnal variations of the fine-mode aerosol mass and ambient RH between the ground level and the 532-m level may explain this. Fig. 5b and e show the diurnal variations in ambient RH at the ground level and at 532 m, respectively. With the relatively uniform water vapor mixing ratio and decreasing temperature with altitude in the PBL (Stull, 1988; Liu and Liang, 2010), the ambient RH at 532 m (ranging from 72% to 78%) was systematically higher than the RH at the surface level (ranging from 35% to 68%). The surface RH had a notable diurnal cycle where the average standard deviation of the surface RH (15%) was much smaller than the variation in RH values (33%), partly linked with the evolution of the PBL. During the development of the PBL, dry and clean air masses are entrained into the PBL (Wallace and Hobbs, 2006). Consequently, the surface RH decreases during the daytime. Different from the surface RH, the ambient RH at 532 m was relatively uniform. The variation in ambient RH values at 532 m (6%) was much less than the average standard deviation (12%). This is because the humidity in most of the middle and upper boundary layer does not change due to diminished turbulence (Stull, 1988). The diurnal variation in RH at 532 m was thus not discernible. The diurnal variation in RH at 532 m is characterized by large standard deviations. Associated with the thermodynamic structure within the PBL, the large difference in ambient RH between the surface level and 532 m would lead to disparities in the ALWC and aerosol optical properties. Fig. 5a and d show the diurnal variations in aerosol mass concentration at the ground level and at 532 m, respectively. The surface $PM_{2.5}$ (ranging from 36 to 52 $\mu g m^{-3}$) was systematically higher than $PM_{2.5}$ at 532 m (ranging from 14 to 21 $\mu g m^{-3}$). Surface $PM_{2.5}$ had a notable diurnal cycle characterized by a valley (36 $\mu g m^{-3}$) during the daytime (1730 LT) and a peak (52 $\mu g m^{-3}$) at night (2000 LT), overall

opposite to what was seen at 532 m. This disparity is also partly related to the evolution of the PBL. Wang et al. (2018) have suggested that newly formed fine particles and their coagulation and growth contribute little to $PM_{2.5}$ due to the small volume of newly formed particles. They also state that the evolution of the PBL has a greater influence on aerosol mass concentration at the surface. Note that the surface observation station is next to the Chang Long Paradise amusement park, surrounded by food stalls that could emit a large number of particles from cooking at night. Accordingly, observed is a notable decline and increase in the fine-mode aerosol mass at the surface during the daytime and in the evening, respectively. On the contrary, a rapid accumulation of fine-mode aerosol particles took place in the morning at 532 m (increasing from 14 to 21 $\mu g m^{-3}$), also partly linked with the diminished turbulence in the middle and upper parts of the boundary layer. In the upper boundary layer, turbulence diminished, thus weakening the impact of the evolution of the PBL on $PM_{2.5}$. Consequently, a sharp increase in $PM_{2.5}$ was observed in the morning due to the considerable number of fine particles created during new-particle-formation events. The diurnal variation in β_p was similar to that in $PM_{2.5}$, based on the relatively uniform RH in the upper boundary layer. Fig. 5c and f show the diurnal variation in aerosol hygroscopicity at the ground level and at 532 m, respectively. Note that the diurnal cycles of κ at the surface and at 532 m are similar, both characterized by a clear peak (0.30 and 0.29, respectively) and valley (0.23 and 0.24, respectively) at 1100 LT and 1900 LT, and 1000 LT and 2000 LT, respectively. Meanwhile, observed were sharp increases in the SO_4^{2-} mass concentration (from 16% to 20%) and the NO_3^- mass concentration (from 12% to 18%) in the morning and evening, as well as a notable increase in Org (from 52% to 62%) in the afternoon (Fig. S11). The sharp increase in κ in the morning is thus likely related to strong photochemical reactions that facilitate the transformation of SO_2 to SO_4^{2-} and NO_x to NO_3^- (Wang et al., 2018). The notable decline in κ in the afternoon results from the considerable number of organic species emitted and formed through oxidation (Zhang et al., 2018). The average maximum and minimum values of aerosol hygroscopicity are both around 0.3 and 0.25, respectively, at the ground level and at 532 m. These results further demonstrate that aerosol chemical species at the ground level and at 532 m were similar.

In summary, the diurnal variations in ambient RH, $PM_{2.5}$, and β_p at the ground level and at 532 m are significantly different from each

other. Associated with the thermodynamic structure within the PBL, the diurnal cycles of ambient RH and $PM_{2.5}$ are both characterized by a clear peak in the afternoon at the surface level. Due to diminished turbulence in the upper boundary layer, the ambient RH there is relatively uniform with no clear diurnal variation, and $PM_{2.5}$ has a diurnal cycle opposite to that at the surface. The noticeable differences in ambient RH and $PM_{2.5}$ between the surface level and the upper boundary layer led to the overall opposite diurnal cycle pattern in β_p .

4.3. The impact of different factors (ambient RH, $PM_{2.5}$, and κ) on aerosol optical properties

4.3.1. Correlation analysis

As previously discussed, the surface RH is significantly different from that in the upper boundary layer. The surface $PM_{2.5}$ is also significantly different from that in the upper boundary layer because of the thermodynamic structure within the PBL, leading to disparities in aerosol optical properties. Therefore, to further investigate the impact of different factors, such as the ambient RH, $PM_{2.5}$, and κ , on β_p and to compare their differences between the surface level and the 532 m level, the correlations between β_p and fine-mode aerosol mass under four different ambient RH conditions and differentiated by κ were analyzed at these two levels.

At the ground level, the coefficients of determination (R^2) between β_p and $PM_{2.5}$ mass concentration are 0.90, 0.92, 0.88, and 0.85 when $RH \leq 60\%$, $60 < RH \leq 70\%$, $70 < RH \leq 80\%$, and $80 < RH \leq 90\%$, respectively (Fig. 6). The surface β_p correlates well with $PM_{2.5}$ mass concentration under all RH conditions, suggesting that fine-mode aerosols were an important factor influencing the variation in aerosol optical properties at the surface. However, β_p at the 532-m level shows a relatively weaker correlation with $PM_{2.5}$ mass concentration ($R^2 < 0.6$) under all ambient RH conditions (Fig. 7). Under low RH conditions ($RH < 70\%$), $PM_{2.5}$ at 532 m ranged from 5 to $60 \mu\text{g m}^{-3}$, values much higher than under high RH conditions, and β_p and $PM_{2.5}$ were better correlated ($R^2 > 0.5$). The surface β_p was much higher, as much as four times greater than that at 532 m. These results suggest that the

impact of aerosol loading on aerosol optical properties at the ground level was more important than that in the upper boundary layer over Guangzhou. Figs. 6 and 7 also show that β_p increased slightly as the fine-mode aerosol mass concentration increased under low RH conditions and increased sharply under high RH conditions both at the ground and 532-m levels. This is likely because there were more SA with higher aerosol hygroscopicities formed under high RH conditions, contributing more to β_p through aerosol hygroscopic growth (Wu et al., 2018; Jin et al., 2020). This illustrates the significant impact of ambient RH on aerosol light scattering. Also, the slopes of the best-fit regression lines at the surface level varied little as the ambient RH increased, ranging from 0.52 to 0.67. At the 532-m level, sharp increases in the slope were seen, ranging from 0.15 to 0.84. Such a difference between the surface and 532 m shows that the impact of ambient RH on aerosol light scattering in the boundary layer is noticeably larger than at the ground level. This is partly related to aerosol size distributions. As shown in Fig. S12, the shapes of the particle size distributions were similar under different RH conditions at the surface, with two peaks at ~ 20 nm and ~ 100 nm. However, under low RH conditions ($RH < 60\%$), the particle size distribution was the broadest in the small-particle size range than under higher RH conditions, with a less clear peak at 100 nm, likely related to the influence of high emissions of smaller particles under low RH conditions from local sources. This explains the different slopes of the $PM_{2.5}$ mass concentration and β_p relations under different RH conditions, with the higher slope associated with higher RH conditions. The potential impacts of the aerosol size distribution on β_p were examined next using Mie scattering theory (Du, 2004; Bohren and Huffman, 2007). $PM_{2.5}$ and κ were first set using their mean values as fixed values. Then based on all PNSD and RH data collected, Mie theory was used to calculate β_p . The average contributions of the particle size distribution to β_p were 8.19%, 7.92%, 7.27%, and 6.52% at $RH = 40\%$, 60%, 80% and 90%, respectively. The influence of the aerosol size distribution on aerosol light scattering was thus relatively small at the same $PM_{2.5}$ mass concentration during the campaign in Guangzhou. Surface β_p increased as κ increased under the same $PM_{2.5}$ and ambient RH conditions (Fig. 6). Moreover, β_p

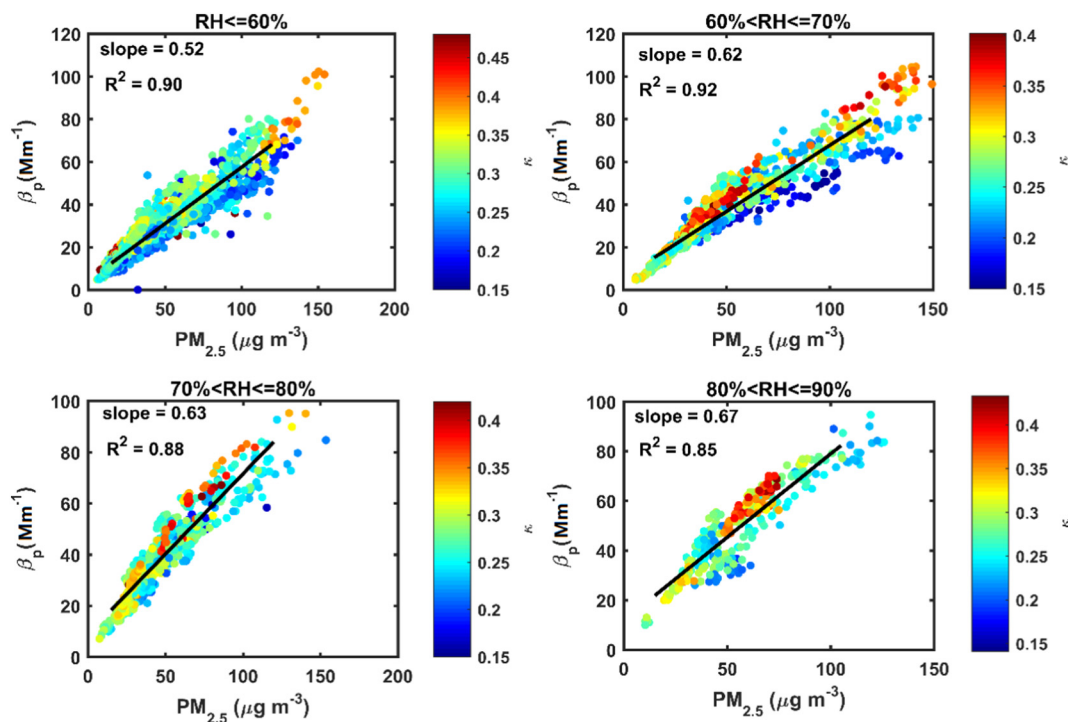


Fig. 6. The correlation between aerosol backscattering coefficient (β_p) and $PM_{2.5}$ mass concentration for four ambient relative humidity (RH) ranges at the ground level. The color of the dots represents the magnitude of the aerosol hygroscopicity parameter (κ). The black lines are the best-fit lines from linear regression. The slopes of the lines and coefficients of determination are given in each panel. (For interpretation of the references to color in this figure legend, the reader is referred to the web version of this article.)

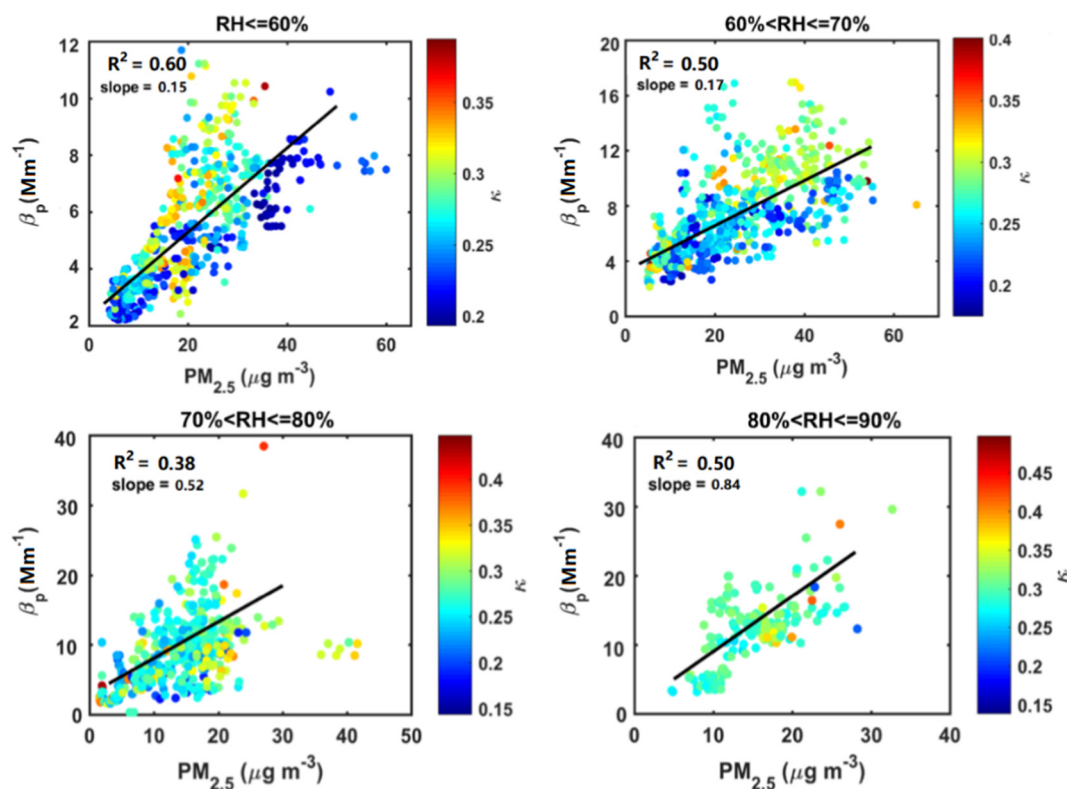


Fig. 7. Same as Fig. 6 except at the 532-m level.

increased more significantly with the enhancement in κ under high $\text{PM}_{2.5}$ mass concentration conditions, related to the large contribution of accumulation-mode particles to aerosol hygroscopic growth. During polluted periods, aerosol particles dominated by accumulation-mode particles are highly aged and can take up considerable liquid water, changing particle sizes. This further increases aerosol light scattering during the evolution of heavy haze episodes, consequently increasing β_p more significantly as κ increases (Swietlicki et al., 1999; Bian et al., 2014). The increase in β_p as κ increases is also seen at 532 m. These results show the notable impact of aerosol hygroscopicity on β_p , especially during heavy haze periods.

In summary, ambient RH, aerosol mass concentration, and aerosol hygroscopicity all influence aerosol optical properties significantly at the ground level and in the upper boundary layer. However, the impacts of the three related factors on β_p are noticeably different between the surface level and the upper boundary layer. The β_p correlates well with $\text{PM}_{2.5}$ at the surface but relatively poorly at 532 m, enhancing slightly as ambient RH increases at the surface but sharply at 532 m.

4.3.2. Sensitivity analysis

As discussed in Section 4.3.1, the ambient RH, aerosol mass concentration, and aerosol hygroscopicity all have significant impacts on aerosol optical properties at the ground level and in the upper boundary layer. However, their impacts on β_p are very different because of the complex interactions between the three related factors (Chen et al., 2014; Ma et al., 2014). As ambient RH increases, aerosols grow through water uptake, further accelerating the formation of SA and particle accumulation, thus enhancing aerosol hygroscopicity and forming a positive feedback (Wu et al., 2018). Therefore, it is important and essential to quantitatively evaluate the impacts of ambient RH, $\text{PM}_{2.5}$ mass concentration, and aerosol hygroscopicity on β_p . Fig. 8 shows the absolute changes in β_p caused by ambient RH, $\text{PM}_{2.5}$ mass concentration, and κ , calculated based on the methods introduced in Section 3.3. The absolute change in β_p has linear relationships with $\text{PM}_{2.5}$ mass concentration and κ at the ground level and at 532 m. The $\text{PM}_{2.5}$ mass concentration increased

by $10 \mu\text{g m}^{-3}$, and β_p increased by 6.5 and 5.2 Mm^{-1} at the ground level and at 532 m, respectively. The standard deviation of the $\text{PM}_{2.5}$ mass concentration at the ground level is much smaller than that at 532 m, partly related to the more significant correlation between β_p and $\text{PM}_{2.5}$ mass concentration at the surface than at 532 m. The parameter κ increased by 0.1, and β_p increased by 6.2 and 6.0 Mm^{-1} at the ground level and at 532 m, respectively. However, the absolute change in β_p has an exponential relationship with ambient RH at both the ground level and at 532 m, similar to the relationship between ALWC and ambient RH (Tan et al., 2017; Jin et al., 2020), indicating the important impact of ALWC on aerosol light scattering through aerosol particle hygroscopic growth. Note that β_p increased more rapidly as the ambient RH increased under relatively low RH conditions at the ground level, while the increase in β_p became sharp under high RH conditions at 532 m, consistent with previous results showing the pronounced increase in the slope at 532 m and the slight increase in the slope at the ground level. This is likely related to the more polluted conditions at the ground level where aerosol particles are mostly composed of accumulation-mode particles, facilitating aerosol hygroscopic growth under relatively low ambient RH conditions, thus increasing β_p (Wu et al., 2018).

Fig. 9 shows the relative contributions of ambient RH, $\text{PM}_{2.5}$ mass concentration, and κ to changes in β_p at the ground level and at 532 m. On average, κ , $\text{PM}_{2.5}$ mass concentration, and ambient RH account for 25%, 42%, and 33%, respectively, at the ground level. This suggests that the impact of the accumulation of aerosol particles themselves on aerosol light scattering is the most important among the three factors, followed by aerosol hygroscopic growth due to the increase in the ambient RH, and finally, the enhancement in κ through multiple-phase chemical reactions. These results imply that local emission controls can decrease β_p significantly, further improving atmospheric visibility effectively at the surface during winter in Guangzhou. At the 532-m level on the tower, aerosol hygroscopicity, $\text{PM}_{2.5}$ mass concentration, and ambient RH accounted for 24%, 30%, and 46%, respectively. The relative contributions of aerosol chemical composition to the variability in

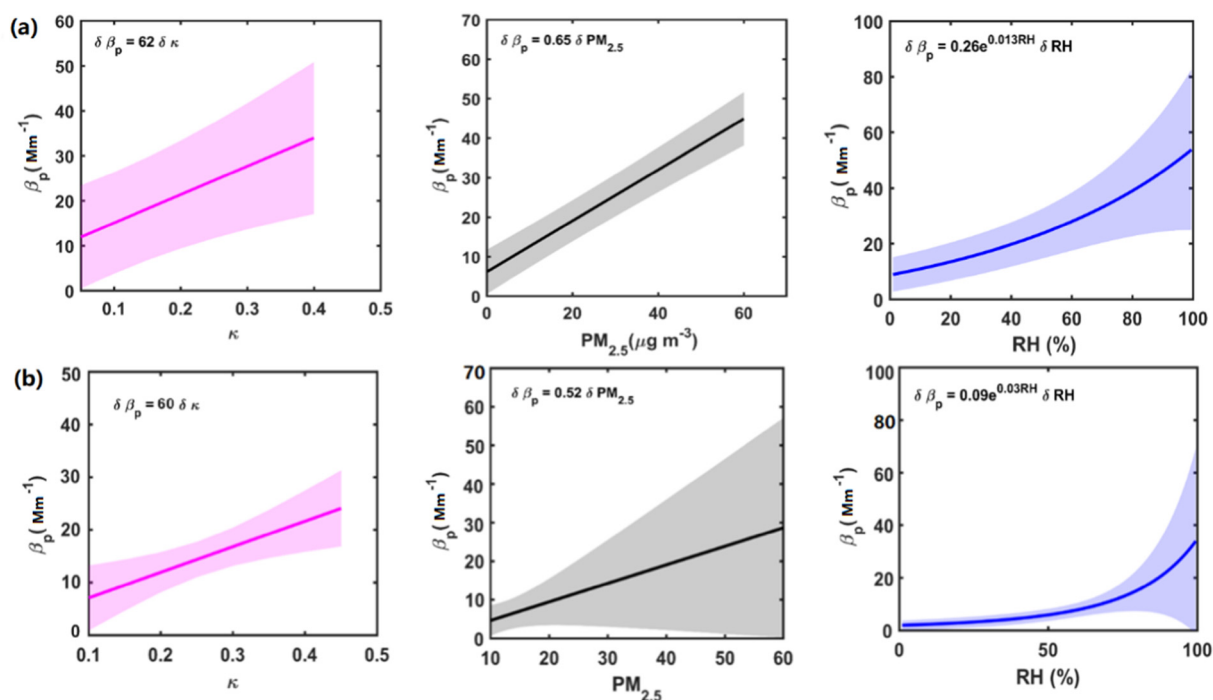


Fig. 8. The absolute change in aerosol backscattering coefficient (β_p) with (from left to right) aerosol hygroscopicity (κ), $PM_{2.5}$ mass concentration, and ambient relative humidity (RH) (a) at the ground level and (b) at 532 m on the tower. Shaded areas represent standard deviations.

β_p at the ground level and at 532 m are generally similar and the smallest among the three factors, indicating that aerosol hygroscopic growth caused by chemical processes played a relatively weaker role in influencing aerosol optical properties at both the ground level and in the upper boundary layer over Guangzhou. Note that the contribution of ambient RH is the largest at 532 m, followed by aerosol mass concentration, different from that at the ground level, indicating that aerosol hygroscopic growth resulting from high ambient RH played a key role in determining aerosol light scattering in the upper boundary layer in winter over Guangzhou.

5. Conclusions

A winter field campaign was carried out at the Guangzhou Meteorological Bureau station in the PRD region of China from 1 November 2019 to 21 January 2020 at the surface level and from 1 February to 21 March 2020 at the nearby Guangzhou tower. Measurements made at 532 m on the tower can generally represent the air quality condition in the upper part of the PBL. The

core issue of haze is light scattering, affected by both pollutants and meteorological factors, especially their variations throughout the boundary layer. Previous studies have chiefly been ground based and less focused on the relative contributions of various factors to aerosol optical properties. This study investigated the relationship between pertinent factors (ambient RH, $PM_{2.5}$, and aerosol hygroscopicity) and aerosol optical properties (aerosol scattering coefficient, β_p) and further compared differences between the ground level and the upper boundary layer.

In general, the temporal variation of β_p was consistent with that of ALWC, and high β_p values were usually associated with correspondingly high ALWC values. The diurnal cycles of ALWC and β_p were similar at the ground level and at 532 m, suggesting that aerosol liquid water plays an important role in light scattering through aerosol hygroscopic growth. There were four main haze events observed during the experiment. The surface $PM_{2.5}$ mass concentration was much higher than that at 532 m. Organics and sulfates were the dominant species in $PM_{2.5}$ both at the ground level (58% and 18%, respectively) and at 532 m (57% and 20%, respectively), showing that the aerosol chemical species at the surface

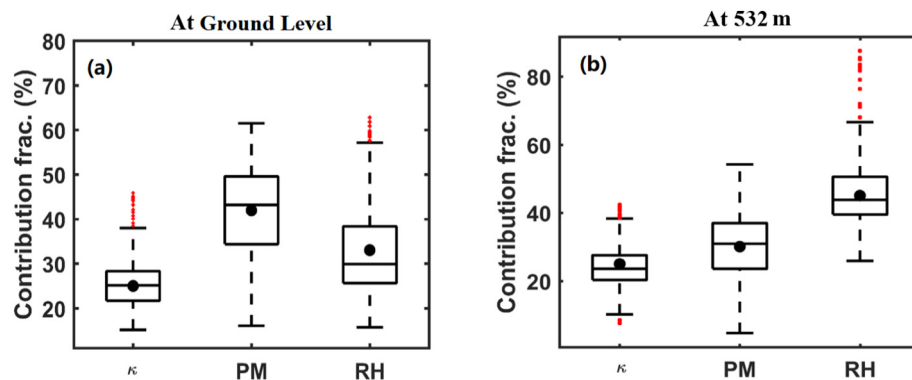


Fig. 9. Mean contribution fractions (black dots) of aerosol hygroscopicity (κ), $PM_{2.5}$ mass concentration, and ambient relative humidity (RH, solid dots), with boxes showing the 25th, 50th, and 75th percentiles (a) at the ground level and (b) at 532 m on the tower. The extremities show the 5th and 95th percentiles, and the red dots show outliers. (For interpretation of the references to color in this figure legend, the reader is referred to the web version of this article.)

and in the upper boundary layer were similar. Associated with the thermodynamic structure within the PBL, the noticeable difference in ambient RH and PM_{2.5} between the surface level and the upper boundary layer was demonstrated. The ambient RH in the upper boundary layer was systematically higher than the surface RH. The ambient RH had a clear diurnal cycle at the surface level and was relatively uniform in the upper boundary layer. The surface PM_{2.5} concentration was systematically higher than that at 532 m, with opposite diurnal cycles. These differences would lead to disparities in aerosol optical properties between the surface and the upper boundary layer.

The ambient RH, aerosol mass concentration, and aerosol hygroscopicity influenced aerosol optical properties significantly, both at the ground level and at 532 m. As β_p increased with increasing ambient RH, the aerosol mass concentration also increased due to the accumulation of particles and secondary aerosol formation, further increasing β_p . The contribution of the particle size distribution to β_p at the same PM_{2.5} level at the surface was also evaluated, with average values of 8.19%, 7.92%, 7.27%, and 6.52% at RH = 40%, 60%, 80%, and 90%, respectively. This suggests that the influence of the aerosol size distribution on aerosol light scattering was small at the same PM_{2.5} mass concentration level during the campaign in Guangzhou. A sensitivity analysis was performed to determine which factor had the most impact on aerosol optical properties at the surface and at 532 m. The clear difference in the sensitivity of aerosol light scattering to the ambient RH, aerosol loading, and aerosol chemical composition between the surface and the upper boundary layer was demonstrated. The relative contributions of aerosol hygroscopicity to the variability in β_p at the surface level (25%) and at 532 m (24%) were the smallest among the three factors, likely linked with the relatively weaker aerosol hygroscopicity and the small variation in aerosol hygroscopicity during the winter experiment in Guangzhou. β_p was more sensitive to PM_{2.5} at the surface level (accounting for 42%) and more sensitive to the ambient RH in the upper boundary layer (accounting for 46%). This is mainly related to the more polluted conditions at the ground level and the higher ambient RH conditions in the upper boundary layer. These results help toward quantitatively understanding the relative contributions of meteorological factors and atmospheric chemical processes to pollution. They also reveal to some degree the causes and measures to take to combat air pollution in China.

CRedit authorship contribution statement

ZL and XJ determined the main goal of this study. XJ carried out the study, analyzed the data, and prepared the paper with contributions from all co-authors. TW, YW, and TS participated in discussions and provided scientific suggestions. TW provided aerosol vertical profile obtained from the PML. HW provided ground weather data, wind profile data, and corresponding technical support. SL provided the aerosol chemical composition measured by the ACSM. RR provided aerosol scattering coefficient data and aerosol light-scattering enhancement factors measured by the nephelometer.

Declaration of competing interest

The authors declare that they have no conflict of interest or personal relationships that could have appeared to influence the work reported in this paper.

Acknowledgements

This work was supported by the Natural Science Foundation of China (NSFC) research project (Grant No. 91544217), the National Key Research and Development Program of China (Grant No. 2017YFC1501702), and the Guangdong Basic and Applied Basic Research Fund (Grant No. 2020B1515130003).

Data availability

Data used in this study are available from the first author upon request by contacting Xiaojin Jin (jinxa12@umd.edu).

Appendix A. Supplementary data

Supplementary data to this article can be found online at <https://doi.org/10.1016/j.scitotenv.2021.150010>.

References

- Bian, Y.X., Zhao, C.S., Ma, N., Chen, J., Xu, W.Y., 2014. A study of aerosol liquid water content based on hygroscopicity measurements at high relative humidity in the North China plain. *Atmos. Chem. Phys.* 14, 6417–6426. <https://doi.org/10.5194/acp-14-6417-2014>.
- Bohren, C.F., Huffman, D.R., 2007. *Absorption and scattering by an arbitrary particle. Absorption and Scattering of Light by Small Particles*. Wiley-VCH, Berlin, pp. 57–81.
- Carbone, S., Saarikoski, S., Frey, A., Reyes, F., Reyes, P., Castillo, M., Gramsch, E., Oyola, P., Jayne, J., Worsnop, D.R., Hillamo, R., 2013. Chemical characterization of submicron aerosol particles in Santiago de Chile. *Aerosol Air Qual. Res.* 13, 462–473. <https://doi.org/10.4209/aaqr.2012.10.0261>.
- Chen, J., Zhao, C.S., Ma, N., Yan, P., 2014. Aerosol hygroscopicity parameter derived from the light scattering enhancement factor measurements in the North China plain. *Atmos. Chem. Phys.* 14 (15), 8105–8118.
- Cheng, Y.F., Eichler, H., Wiedensohler, A., Heintzenberg, J., Zhang, Y.H., Hu, M., Herrmann, H., Zeng, L.M., Liu, S., Gnauk, T., Brüggemann, E., He, L.Y., 2006. Mixing state of elemental carbon and non-light-absorbing aerosol components derived from in situ particle optical properties at xinken in Pearl River Delta of China. *J. Geophys. Res. Atmos.* 111. <https://doi.org/10.1029/2005JD006929>.
- Cheng, Y.F., Wiedensohler, A., Eichler, H., Heintzenberg, J., Tesche, M., Ansmann, A., Wendisch, M., Su, H., Althausen, D., Herrmann, H., Gnauk, T., Brüggemann, E., Hu, M., Zhang, Y.H., 2008a. Relative humidity dependence of aerosol optical properties and direct radiative forcing in the surface boundary layer at xinken in Pearl River Delta of China: an observation based numerical study. *Atmos. Environ.* 42, 6373–6397. <https://doi.org/10.1016/j.atmosenv.2008.04.009>.
- Cheng, Y.F., Wiedensohler, A., Eichler, H., Su, H., Gnauk, T., Brüggemann, E., Herrmann, H., Heintzenberg, J., Slanina, J., Tuch, T., Hu, M., Zhang, Y.H., 2008b. Aerosol optical properties and related chemical apportionment at xinken in Pearl River Delta of China. *Atmos. Environ.* 42, 6351–6372. <https://doi.org/10.1016/j.atmosenv.2008.02.034>.
- Cheng, Y., Zheng, G., Wei, C., Mu, Q., Zheng, B., Wang, Z., Gao, M., Zhang, Q., He, K., Carmichael, G., Pöschl, U., Su, H., 2016. Reactive nitrogen chemistry in aerosol water as a source of sulfate during haze events in China. *Sci. Adv.* 2, e1601530. <https://doi.org/10.1126/sciadv.1601530>.
- Covert, D.S., Charlson, R.J., Ahlquist, N.C., 1972. A study of the relationship of chemical composition and humidity to light scattering by aerosols. *J. Appl. Meteorol.* 11 (6), 968–976.
- Cui, J., Shi, T., Zhou, Y., Wu, D., Wang, X., Pu, W., 2021. Satellite-based radiative forcing by light-absorbing particles in snow across the northern hemisphere. *Atmos. Chem. Phys.* 21, 269–288. <https://doi.org/10.5194/acp-21-269-2021>.
- Deng, T., Wu, D., Deng, X., Tan, H., Li, F., Liao, B., 2014. A vertical sounding of severe haze process in Guangzhou area. *Sci. China Earth Sci.* 57 (11), 2650–2656.
- Ding, A.J., Huang, X., Nie, W., Sun, J.N., Kerminen, V.M., Petäjä, T., Su, H., Cheng, Y.F., Yang, X.Q., Wang, M.H., Chi, X.G., 2016. Enhanced haze pollution by black carbon in megacities in China. *Geophys. Res. Lett.* 43, 2873–2879.
- Du, H., 2004. Mie-scattering calculation. *Appl. Opt.* 43 (9), 1951–1956.
- Fan, J., Rosenfeld, D., Zhang, Y., Giangrande, S.E., Li, Z., 2018. Substantial convection and precipitation enhancements by ultrafine aerosol particles. *Science* 359, 411–418. <https://doi.org/10.1126/science.aan8461>.
- Fountoukis, C., Nenes, A., 2007. ISORROPIA II: a computationally efficient thermodynamic equilibrium model for K–Ca2–Mg2–NH4–Na–SONO–Cl–H2O aerosols. *Atmos. Chem. Phys.* 7, 4639–4659. <https://doi.org/10.5194/acp-7-4639-2007>.
- Gobbi, G.P., Barnaba, F., Van Dingenen, R., Putaud, J.P., Mircea, M., Facchini, M.C., 2003. Lidar and in situ observations of continental and saharan aerosol: closure analysis of particles optical and physical properties. *Atmos. Chem. Phys.* 3, 2161–2172. <https://doi.org/10.5194/acp-3-2161-2003>.
- Guo, J., Miao, Y., Zhang, Y., Liu, H., Li, Z., Zhang, W., He, J., Lou, M., Yan, Y., Bian, L., Zhai, P., 2016. The climatology of planetary boundary layer height in China derived from radiosonde and reanalysis data. *Atmos. Chem. Phys.* 16 (20), 13309–13319.
- Guo, J., Su, T., Li, Z., Miao, Y., Li, J., Liu, H., Xu, H., Cribb, M., Zhai, P., 2017. Declining frequency of summertime local-scale precipitation over eastern China from 1970 to 2010 and its potential link to aerosols. *Geophys. Res. Lett.* 44 (11), 5700–5708.
- Guo, J., Su, T., Chen, D., Wang, J., Li, Z., Lv, Y., Guo, X., Liu, H., Cribb, M., Zhai, P., 2019. Declining summertime local-scale precipitation frequency over China and the United States, 1981–2012: the disparate roles of aerosols. *Geophys. Res. Lett.* 46 (22), 13281–13289.
- Gysel, M., Grosjean, J., Topping, D.O., Whitehead, J.D., Bower, J.N., Cubison, M.J., Williams, P.I., Flynn, M.J., McFiggans, G.B., Coe, H., 2007. Closure study between chemical composition and hygroscopic growth of aerosol particles during TORCH2. *Atmos. Chem. Phys.* 7, 6131–6144. <https://doi.org/10.5194/acp-7-6131-2007>.
- Hennigan, C.J., Bergin, M.H., Dibb, J.E., Weber, R.J., 2008. Enhanced secondary organic aerosol formation due to water uptake by fine particles. *Geophys. Res. Lett.* 35, L18801. <https://doi.org/10.1029/2008GL035046>.

- Hu, D., Liu, D., Zhao, D., Yu, C., Liu, Q., Tian, P., et al., 2020. Closure investigation on cloud condensation nuclei ability of processed anthropogenic aerosols. *J. Geophys. Res. Atmos.* 125, e2020JD032680.
- Hu, D., Wang, Y., Yu, C., Xie, Q., Yue, S., Shang, D., et al., 2021. Vertical profile of particle hygroscopicity and CCN effectiveness during winter in Beijing: insight into the hygroscopicity transition threshold of black carbon. *Faraday Discuss.* 226, 239–254. <https://doi.org/10.1039/D0FD00077A>.
- Huang, J., Yi, Y., 1991. Inversion of a nonlinear dynamical model from the observation. *Sci. China B* 10.
- Huang, Z., Huang, J., Bi, J., Wang, G., Wang, W., Fu, Q., Li, Z., Tsay, S.-C., Shi, J., 2010. Dust aerosol vertical structure measurements using three MPL lidars during 2008 China-U.S. joint dust field experiment. *J. Geophys. Res. Atmos.* 115, D00K15.
- Huang, R.J., Zhang, Y., Bozzetti, C., Ho, K.F., Cao, J.J., Han, Y., Daellenbach, K.R., Slowik, J.G., Platt, S.M., Canonaco, F., Zotter, P., 2014. High secondary aerosol contribution to particulate pollution during haze events in China. *Nature* 514 (7521), 218–222.
- IPCC, 2013. *Climate change 2013: scientific basis. Fifth Assessment of the Intergovernmental Panel on Climate Change.* Cambridge University Press.
- Jimenez, J.L., Jayne, J.T., Shi, Q., Kolb, C.E., Worsnop, D.R., Yourshaw, L., Morris, J.W., 2003. Ambient aerosol sampling using the aerodyne aerosol mass spectrometer. *J. Geophys. Res. Atmos.* 108, 8425. <https://doi.org/10.1029/2001JD001213>.
- Jin, X., Wang, Y., Li, Z., Zhang, F., Xu, W., Sun, Y., Fan, X., Chen, G., Wu, H., Ren, J., Wang, Q., 2020. Significant contribution of organics to aerosol liquid water content in winter in Beijing. *China. Atmos. Chem. Phys.* 20 (2), 901–914.
- Kuang, Y., Zhao, C.S., Tao, J.C., Bian, Y.X., Ma, N.J.A.E., 2016. Impact of aerosol hygroscopic growth on the direct aerosol radiative effect in summer on North China plain. *Atmos. Environ.* 147, 224–233.
- Levin, E.J.T., Prenni, A.J., Palm, B.B., Day, D.A., Campuzano-Jost, P., Winkler, P.M., Kreidenweis, S.M., DeMott, P.J., Jimenez, J.L., Smith, J.N., 2014. Size-resolved aerosol composition and its link to hygroscopicity at a forested site in Colorado. *Atmos. Chem. Phys.* 14 (5), 2657–2667.
- Li, Z., Lau, W.M., Ramanathan, V., Wu, G., Ding, Y., Manoj, M.G., Liu, J., Qian, Y., Li, J., Zhou, T., 2016. Aerosol and monsoon climate interactions over Asia. *Rev. Geophys.* 54, 866–929. <https://doi.org/10.1002/2015RG000500>.
- Liu, S., Liang, X.-Z., 2010. Observed diurnal cycle climatology of planetary boundary layer height. *J. Clim.* 22, 5790–5809. <https://doi.org/10.1175/2010JCLI3552.1>.
- Ma, N., Zhao, C., Chen, J., Xu, W., Yan, P., Zhou, X., 2014. A novel method for distinguishing fog and haze based on PM_{2.5}, visibility, and relative humidity. *Sci. China: Earth Sci.* 57, 2156–2164.
- Malm, W.C., McMeeking, G.R., Kreidenweis, S.M., Levin, E., Carrico, C.M., Day, D.E., Collett, J.L., Lee, T., Sullivan, A.P., Raja, S., 2009. Using high time resolution aerosol and number size distribution measurements to estimate atmospheric extinction. *J. Air Waste Manage. Assoc.* 59, 1049–1060. <https://doi.org/10.3155/1047-3289.59.9.1049>.
- Martin, S.T., 2000. Phase transitions of aqueous atmospheric particles. *Chem. Rev.* 100, 3403–3454. <https://doi.org/10.1021/cr990034t>.
- Ng, N.L., Herndon, S.C., Trimborn, A., Canagaratna, M.R., Croteau, P.L., Onasch, T.B., Sueper, D., Worsnop, D.R., Zhang, Q., Sun, Y.L., Jayne, J.T., 2011. An aerosol chemical speciation monitor (ACSM) for routine monitoring of the composition and mass concentrations of ambient aerosol. *Aerosol Sci. Technol.* 45, 780–794. <https://doi.org/10.1080/02786826.2011.560211>.
- Nguyen, T.K.V., Zhang, Q., Jimenez, J.L., Pike, M., Carlton, A.G., 2016. Liquid water: ubiquitous contributor to aerosol mass. *Environ. Sci. Technol. Lett.* 3 (7), 257–263.
- Nilsson, E.D., Rannik, Ü., Kumala, M., Buzorius, G., O'Dowd, C.D., 2001. Effects of continental boundary layer evolution, convection, turbulence and entrainment, on aerosol formation. *Tellus Ser. B Chem. Phys. Meteorol.* 53 (4), 441–461.
- Petters, M.D., Kreidenweis, S.M., 2007. A single parameter representation of hygroscopic growth and cloud condensation nucleus activity. *Atmos. Chem. Phys.* 7, 1961–1971. <https://doi.org/10.5194/acp-7-1961-2007>.
- Pierangelo, C., Chedin, A., Heilliette, S., Jacquinet-Husson, N., Armante, R., 2004. Dust altitude and infrared optical depth from AIRS. *Atmos. Chem. Phys.* 4, 1813–1822. <https://doi.org/10.5194/acp-4-1813-2004>.
- Seinfeld, H.J., Pandis, N.S., 2006. *Atmospheric Chemistry and Physics: From Air Pollution to Climate Change.* John Wiley & Sons <https://doi.org/10.1080/00139157.1999.10544295>.
- Stokes, R.H., Robinson, R.A., 1966. Interactions in aqueous nonelectrolyte solutions. I. Solute-solvent equilibria. *J. Phys. Chem.* 70, 2126–2131. <https://doi.org/10.1021/j100879a010>.
- Stull, R.B., 1988. *An Introduction to Boundary Layer Meteorology.* Kluwer Academic Publishers.
- Su, T., Li, J., Li, C., Xiang, P., Lau, A.K.H., Guo, J., Yang, D., Miao, Y., 2017. An intercomparison of long-term planetary boundary layer heights retrieved from CALIPSO, ground-based lidar, and radiosonde measurements over Hong Kong. *J. Geophys. Res. Atmos.* 122 (7), 3929–3943.
- Su, T., Li, Z., Kahn, R., 2018. Relationships between the planetary boundary layer height and surface pollutants derived from lidar observations over China: regional pattern and influencing factors. *Atmos. Chem. Phys.* 18 (21), 15921–15935.
- Su, H., Cheng, Y., Pöschl, U., 2020. New multiphase chemical processes influencing atmospheric aerosols, air quality, and climate in the Anthropocene. *ActaQRqweerwq. Chem. Res.* 53 (10), 2034–2043.
- Su, T., Li, Z., Zheng, Y., Luan, Q., Guo, J., 2020a. Abnormally shallow boundary layer associated with severe air pollution during the COVID-19 lockdown in China. *Geophys. Res. Lett.* 47, e2020GL090041. <https://doi.org/10.1029/2020GL090041>.
- Su, T., Li, Z., Li, C., Li, J., Han, W., Shen, C., Tan, W., Wei, J., Guo, J., 2020b. The significant impact of aerosol vertical structure on lower atmosphere stability and its critical role in aerosol–planetary boundary layer (PBL) interactions. *Atmos. Chem. Phys.* 20 (6), 3713–3724.
- Sun, Y., Wang, Z., Dong, H., Yang, T., Li, J., Pan, X., Chen, P., Jayne, J.T., 2012. Characterization of summer organic and inorganic aerosols in Beijing, China with an aerosol chemical speciation monitor. *Atmos. Environ.* 51, 250–259. <https://doi.org/10.1016/j.atmosenv.2012.01.013>.
- Surratt, J.D., Kroll, J.H., Kleindienst, T.E., Edney, E.O., Claeys, M., Sorooshian, A., Ng, N.L., Offenberg, J.H., Lewandowski, M., Jaoui, M., Flagan, R.C., Seinfeld, J.H., 2007. Evidence for organosulfates in secondary organic aerosol. *Environ. Sci. Technol.* 41, 517–527. <https://doi.org/10.1021/es062081q>.
- Swietlicki, E., Zhou, J., Berg, O.H., Martinsson, B.G., Frank, G., Cederfelt, S.I., Dusek, U., Berner, A., Birmili, W., Wiedensohler, A., Yuskiewicz, B., Bower, K.N., 1999. A closure study of bimicrometer aerosol particle hygroscopic behavior. *Atmos. Res.* 50, 205–240. [https://doi.org/10.1016/S0169-8095\(98\)00105-7](https://doi.org/10.1016/S0169-8095(98)00105-7).
- Tan, H., Cai, M., Fan, Q., Liu, L., Li, F., Chan, P.W., Deng, X., Wu, D., 2017. An analysis of aerosol liquid water content and related impact factors in Pearl River Delta. *Sci. Total Environ.* 579, 1822–1830. <https://doi.org/10.1016/j.scitotenv.2016.11.167>.
- Tao, W.K., Chen, J.P., Li, Z., Wang, C., Zhang, C., 2012. Impact of aerosols on convective clouds and precipitation. *Rev. Geophys.* 50, 1–62. <https://doi.org/10.1029/2011RG000369>.
- Tao, J.C., Zhao, C.S., Ma, N., Liu, P.F., 2014. The impact of aerosol hygroscopic growth on the single-scattering albedo and its application on the NO₂ photolysis rate coefficient. *Atmos. Chem. Phys.* 14, 12055e12067.
- Venzac, H., Sellegri, K., Villani, P., Picard, D., Laj, P., 2009. Seasonal variation of aerosol size distributions in the free troposphere and residual layer at the Puy de Dôme station, France. *Atmos. Chem. Phys.* 9 (4), 1465–1478.
- Wallace, J.M., Hobbs, P.V., 2006. *Atmospheric Science: An Introductory Survey.* Vol. 92. Elsevier.
- Wang, S.G., Wang, J.Y., Zhou, Z.J., Shang, K.Z., 2005. Regional characteristics of three kinds of dust storm events in China. *Atmos. Environ.* 39, 509–520.
- Wang, G., Zhang, R., Gomez, M.E., Yang, L., Zamora, M.L., Hu, M., Lin, Y., Peng, J., Guo, S., Meng, J., Li, J., 2016. Persistent sulfate formation from London fog to chinese haze. *Proc. Natl. Acad. Sci. U. S. A.* 113 (48), 13630–13635.
- Wang, Y., Zhang, F., Li, Z., Tan, H., Xu, H., Ren, J., Zhao, J., Du, W., Sun, Y., 2017. Enhanced hydrophobicity and volatility of submicron aerosols under severe emission control conditions in Beijing. *Atmos. Chem. Phys.* 17, 5239–5251. <https://doi.org/10.5194/acp-17-5239-2017>.
- Wang, Y., Li, Z., Zhang, Y., Du, W., Zhang, F., Tan, H., Xu, H., Fan, T., Jin, X., Fan, X., Dong, Z., Wang, Q., Sun, Y., 2018. Characterization of aerosol hygroscopicity, mixing state, and CCN activity at a suburban site in the central North China plain. *Atmos. Chem. Phys.* 18, 11739–11752. <https://doi.org/10.5194/acp-18-11739-2018>.
- Wehner, B., Birmili, W., Ditas, F., Wu, Z., Hu, M., Liu, X., Mao, J., Sugimoto, N., Wiedensohler, A., 2008. Relationships between sub-micrometer particulate air pollution and air mass history in Beijing, China, 2004–2006. *Atmos. Chem. Phys.* 8, 6155–6168. <https://doi.org/10.5194/acp-8-6155-2008>.
- Wei, J., Li, Z., Lyapustin, A., Sun, L., Peng, Y., Xue, W., Su, T., Cribb, M., 2021. Reconstructing 1-km-resolution high-quality PM_{2.5} data records from 2000 to 2018 in China: spatio-temporal variations and policy implications. *Remote Sens. Environ.* 252, 112136. <https://doi.org/10.1016/j.rse.2020.112136>.
- Wex, H., Petters, M.D., Carrico, C.M., Hallbauer, E., Massling, A., McMeeking, G.R., Poulain, L., Wu, Z., Kreidenweis, S.M., Stratmann, F., 2009. Towards closing the gap between hygroscopic growth and activation for secondary organic aerosol: part 1 - evidence from measurements. *Atmos. Chem. Phys.* 9, 3987–3997.
- Wu, Z., Wang, Y., Tan, T., Zhu, Y., Li, M., Shang, D., Wang, H., Lu, K., Guo, S., Zeng, L., Zhang, Y., 2018. Aerosol liquid water driven by anthropogenic inorganic salts: implying its key role in the haze formation over North China plain. *Environ. Sci. Tech. Lett.* 5, 160–166. <https://doi.org/10.1021/acs.estlett.8b00021>.
- Wu, T., Li, Z., Chen, J., Wang, Y., Wu, H., Jin, X.A., Liang, C., Li, S., Wang, W., Cribb, M., 2020. Hygroscopicity of different types of aerosol particles: case studies using multi-instrument data in megacity Beijing, China. *Remote Sens.* 12 (5), 785.
- Yang, D., Li, C., Lau, A.K.H., Li, Y., 2013. Long-term measurement of daytime atmospheric mixing layer height over Hong Kong. *J. Geophys. Res. Atmos.* 118 (5), 2422–2433.
- Yoon, S.C., Kim, J., 2006. Influences of relative humidity on aerosol optical properties and aerosol radiative forcing during ACE-Asia. *Atmos. Environ.* 40, 4328e4338.
- Zhang, L., Cao, X., Bao, J., Zhou, B., Huang, J., Shi, J., Bi, J., 2010. A case study of dust aerosol radiative properties over Lanzhou, China. *Atmos. Chem. Phys.* 10 (9), 4283–4293.
- Zhang, Y., Du, W., Wang, Y., Wang, Q., Wang, H., Zheng, H., Zhang, F., Shi, H., Bian, Y., Han, Y., Fu, P., Canonaco, F., Prévôt, A.S.H., Zhu, T., Wang, P., Li, Z., Sun, Y., 2018. Aerosol chemistry and particle growth events at an urban downwind site in the North China Plain. *Atmos. Chem. Phys. Discuss.* <https://doi.org/10.5194/acp-2017-889>.
- Zheng, G.J., Duan, F.K., Su, H., Ma, Y.L., Cheng, Y., Zheng, B., Zhang, Q., Huang, T., Kimoto, T., Chang, D., Pöschl, U., Cheng, Y.F., He, K.B., 2015. Exploring the severe winter haze in Beijing: the impact of synoptic weather, regional transport and heterogeneous reactions. *Atmos. Chem. Phys.* 15, 2969–2983. <https://doi.org/10.5194/acp-15-2969-2015>.
- Zhou, M., Zhang, L., Chen, D., Gu, Y., Fu, T.M., Gao, M., Zhao, Y., Lu, X., Zhao, B., 2018. The impact of aerosol-radiation interactions on the effectiveness of emission control measures. *Environ. Res. Lett.* 14, 024002. <https://doi.org/10.1088/1748-9326/aaf27d>.
- Zieger, P., Fierz-Schmidhauser, R., Weingartner, E., Baltensperger, U., 2013. Effects of relative humidity on aerosol light scattering: results from different European sites. *Atmos. Chem. Phys.* 13, 10609e10631.
- Zieger, P., Väisänen, O., Corbin, J.C., Partridge, D.G., Bastelberger, S., Mousavi-Fard, M., Rosati, B., Gysel, M., Krieger, U.K., Leck, C., Nenes, A., Riipinen, I., Virtanen, A., Salter, M.E., 2017. Revising the hygroscopicity of inorganic sea salt particles. *Nat. Commun.* 8, 15883. <https://doi.org/10.1038/ncomms15883>.